Tensile Behavior and Morphology Studies of Glass-Fiber-Reinforced Polymeric *In Situ* Hybrid Composites

Hua Liu,[1] Kin Liao[2]

[1]*Department of Mechanical Engineering, Northwestern University, Evanston, Illinois 60208-3111*
[2]*School of Mechanical and Production Engineering, Nanyang Technological University, Singapore 639798*

Received 24 July 2003; accepted 29 March 2004
DOI 10.1002/app.20862
Published online in Wiley InterScience (www.interscience.wiley.com).

ABSTRACT: The morphology and tensile behavior of an *in situ* hybrid composite system, based on E-glass-fibers, liquid-crystalline polymers, and Noryl (a modified polyphenylene ether/polystyrene blend) with a hierarchical microstructure containing reinforcements with an order-of-magnitude difference in size, were studied. The primary reinforcement was short E-glass fibers, and the secondary reinforcement was formed by LCP inclusions with submicrometer dimensions generated *in situ* during fabrication. With an increase in the LCP content, both the geometry and dimensions of the LCP phase in the composites changed, from spherical droplets to ellipsoidal droplets and then to fibrils or lamellar structures. The orientation of the short E-glass fibers was influenced by this change, and the breakage of the glass fibers during processing was less intensive. The tensile strength of the composites increased moderately with the addition of LCPs and the reduction of the glass-fiber content. The elastic modulus of the composites did not follow rule-of-mixture predictions. This more complicated hybrid effect was attributed to several competing mechanisms. Tensile fractography analysis indicated that the tensile fracture of the composites was dominated by fiber/matrix-interface failure. J Appl Polym Sci 94: 211–221, 2004

Key words: composites; liquid-crystalline polymers (LCP); mechanical properties

INTRODUCTION

Over the past several decades, there has been continuing interest in the design and understanding of the fundamental mechanisms that govern the behaviors of hybrid composites, which are material systems made through the incorporation of two or more different types of reinforcements in one or more matrices.[1,2] *In situ* composites, formed by matrices reinforced by inclusions formed *in situ*, have also received considerable attention in recent years. Examples include thermoplastics reinforced microscopically by thermotropic liquid-crystalline polymer (TLCP) fibrils generated *in situ* during the melt processing of blend systems. Combining the concepts of hybrid composites and *in situ* composites has led to novel material systems of *in situ* hybrid composites.[3,4] *In situ* hybrid composites have a unique hierarchical structure consisting of two or more levels of reinforcements of different magnitudes in size. One level of reinforcement is a microscopic fiber, such as glass, carbon, or aramid, whereas the other is submicroscopic TLCP fibrils. Microscopic fibers are mixed with the matrix in their fibrous form before fabrication, whereas TLCP fibrils are generated *in situ* during the melt processing of ternary blends.

The original purpose of adding TLCP to a polymer matrix was to reduce fiber breakage during the processing of short-fiber-reinforced polymeric composites. In most common short-fiber-reinforced polymeric composites, the fiber length is around 3 mm before processing, but it is shortened after processing, especially in the case of injection molding, in which high shear stresses are applied to the melt, breaking the fibers. This fiber breakage reduces the average aspect ratio of the fibers and, therefore, impairs the reinforcing effect of the fibers and the performance of the composites. This phenomenon intensifies with an increase in the viscosity of the melt, which most of the time is induced by an increase in the fiber content. Studies have shown that the addition of TLCP reduces the viscosity of melting blends, and it follows that the addition of TLCP to short-fiber-reinforced composites may reduce the viscosity of the systems and, therefore, relax fiber breakage.[3] Previous studies have also reported that with the addition of TLCP, not only was the original goal of reducing fiber breakage achieved, but the orientation distribution of the microscopic fibers was also altered in a manner favor-

Correspondence to: K. Liao (askliao@ntu.edu.sg).
Contract grant sponsor: Nanyang Technological University (through a research scholarship to H. Liu).

TABLE I
Processing Parameters for Extrusion

Feeding temperature	300°C
Barrel temperature	300°C
Die temperature	230°C
Material feeding speed	0.5–1 rpm
Screw speed	25–27 rpm

ing the realization of their potential reinforcing ability, and the reinforcing effects of the TLCP phases themselves were enhanced.[5,6] Thus, the mechanical properties of hybrid composites have been observed to increase substantially in comparison with those of their parent composites, that is, short-fiber-reinforced composites and *in situ* composites.

In addition to the enhancement of the mechanical properties, these novel composite materials inherit many other desirable characteristics from their parent composites; for instance, the mass production of components with quite intricate shapes is possible. A combination of all the aforementioned advantages makes *in situ* hybrid composites potentially promising candidates for a broad spectrum of engineering applications. However, their fundamental mechanical behaviors have yet to be studied systematically, and little work has been done to date to determine the correlation between their unique structures and mechanical properties. The purpose of this work was to study the morphology and mechanical properties, and the correlation between the two, of an *in situ* hybrid composite system based on E-glass fibers, liquid-crystalline polymers (LCPs), and Noryl (a modified polyphenylene ether/polystyrene blend). Unlike previous works on *in situ* hybrids, this study used relatively low (<10 wt %) LCP weight fractions because we were particularly interested in the effect of adding LCP on the load-bearing capacity of the microscopic reinforcements, not the effect of the LCP inclusion itself as a primary load bearer.

EXPERIMENTAL

Materials

E-glass fibers with a specific gravity of 2.55 g/cm^3, a tensile strength of 1.47–1.96 GPa, Young's modulus of 72.5 GPa, and a maximum elongation of 3% were used. The LCP was Vectra A950 from Ticona, Shelby, NC. Vectra A950 is a commercial, wholly aromatic copolyester with 73% hydroxybenzoate and 27% hydroxy-2-naphthanoate; its glass-transition temperature is 100°C, and its crystalline-solid-to-nematic-liquid transition is 280°C, as determined by differential scanning calorimetry. The matrix material was Noryl 731H from GE Plastics, Selkirk, NY. Noryl is a completely miscible blend of 50% poly(phenylene ether) and 50% polystyrene.

Processing

All the constituent materials were dried in a vacuum oven at 100°C for at least 7 h. Dried materials of predetermined weight fractions were sealed in a plastic bag and tumbled several times for thorough mixing. The following material compositions were used in this study:

- N8G2: 800 g of Noryl (80 wt %) and 200 g of E-glass fibers (20 wt %).
- N8G2L0.2: 800 g of Noryl (78.43 wt %), 200 g of E-glass fibers (19.61 wt %), and 20 g of Vectra A950 (1.96 wt %).
- N8G2L0.5: 800 g of Noryl (76.19 wt %), 200 g of E-glass fibers (19.05 wt %), and 50 g of Vectra A950 (4.76 wt %).
- N8G2L1: 800 g of Noryl (72.73 wt %), 200 g of E-glass fibers (18.18 wt %), and 100 g of Vectra A950 (9.09 wt %).

These materials were subjected to extrusion and injection molding with appropriate processing parameters. The extrusion was performed on a twin-screw ex-

TABLE II
Processing Parameters for Injection Molding

Hopper temperature	130°C (unstable, affected by the other heat zones)
Nozzle temperature	280°C (set according to the Vectra A950 glass-transition temperature)
Barrel temperature	280°C (set according to the Vectra A950 glass-transition temperature)
Dwell	
Pressure	55% of 1068 bar
Speed	55% of 140 rpm
Injection	
Pressure	Full pressure (99.9% of 1068 bar)
Speed	Full speed (99.9% of 140 rpm)
Cycle time	
Clamp	30 s
Injection	7 s

truder from Leistritz Extruder (Somerville, NJ). The processing parameters are listed in Table I. These parameters were extremely important because the processing conditions seriously affected the morphology and, therefore, the mechanical properties of the products.

According to He et al.,[4,6] drawing facilitates the coalescence of LCP droplets and accelerates LCP fibril formation around glass fibers. However, the precise control of the process is a challenge. Therefore, no drawing was applied when the extrudates were squeezed out of the nozzle and water-quenched. The wirelike extrudates were cut into small granules with a rotating cutting machine. The compounded pellets were then dried in vacuum ovens at 100°C for 7 h and stored in sealed plastic bags for subsequent injection molding. Injection molding was performed on a Manumold 77/30 (Manumold, Aylesbury, UK). The parameters are listed in Table II.

Glass-fiber length and orientation

To inspect the glass-fiber length distributions, we placed the injection-molded parts into a furnace, the temperature of which was raised from room temperature at a heating rate of 18°C/min to 450°C and was maintained at that temperature for 1 h. The remnant was immersed in toluene for 4 h. The solution was then centrifuged to separate the dissolved matrix residues, remaining LCP, and suspended glass fibers. After a round, the supernatant liquid was decanted. The remaining solution was immersed in fresh solvent and centrifuged again. These procedures were repeated twice to ensure the cleaning of the matrix and LCP before the final solution was decanted. The substance remaining at the bottom was immersed in ethanol. Drops of ethanol with suspended glass fibers were dropped onto filter paper. After the ethanol evaporated, the paper was coated with gold and examined with scanning electron microscopy (SEM). The length of 100 fibers from each composition was measured to establish the fiber length distribution.

To acquire the in-plane (parallel to the material flow direction and perpendicular to the specimen cross section) orientation distribution of E-glass fibers, we carefully polished and inspected with SEM small sections of the as-received injection-molded parts. The angles between the fiber axes and the material flow direction were measured. The orientations of 40 fibers were measured for each composition.

Testing

To examine the microstructures of the samples without seriously deforming them, we performed cryogenic fractures. The injection-molded parts were immersed in liquid nitrogen for 2 min and were then broken manually. The fracture surfaces were examined with an SEM instrument after they were coated with gold with an SPI module sputter (Structure Probe, Inc. West Chester, PA).

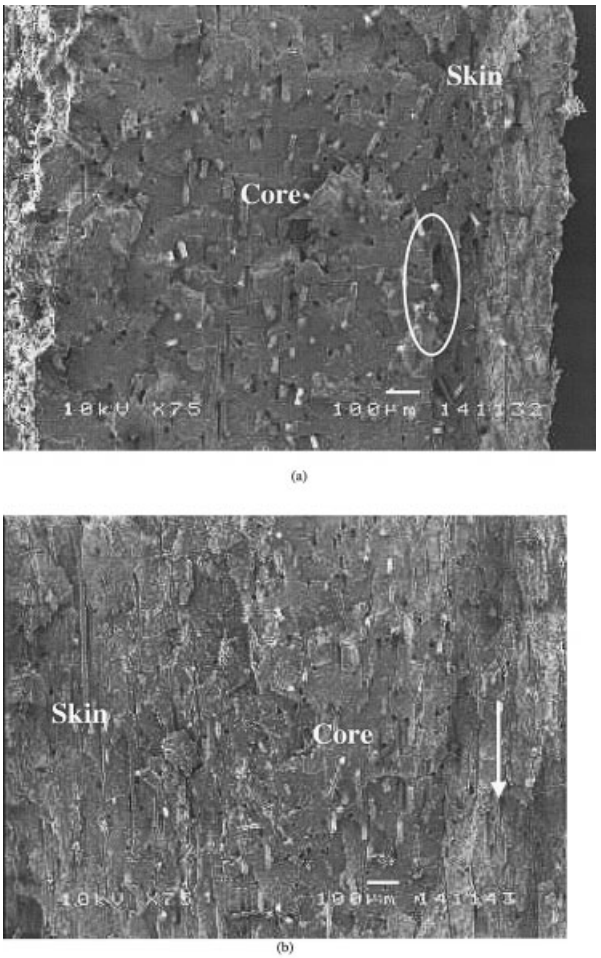

Figure 1 SEM images of the cryogenically fractured surface of N8G2L0.5. (a) The flow direction is perpendicular to the paper plane, and the thermal-shock-induced matrix cracks are marked with a white oval. (b) The flow direction is indicated by the arrow.

To prepare coupons for tensile testing, we cut injection-molded plaques along the longitudinal direction (flow direction) into small, straight-sided tensile coupons (80 mm × 8 mm × 2 mm) with a diamond wheel. The edges of the specimens were polished with silicon carbide papers to remove sharp notches. Glass-woven printed-circuit-board end tabs (20 mm long), with their ends tapered at about 45°, were bonded to the specimen ends with Epicote 600 epoxy (Shell Chemicals, London, UK) or UHU adhesive (Saunders Manufacturing, Winthrop, ME) and were cured under light pressure for at least 24 h before the testing at 16°C. The gauge length of the samples was 40 mm.

All the tensile tests were performed on an Instron 5567 tensile tester (Instron Corporation, Canton, MA) with a ±30 kN static load cell. An Instron

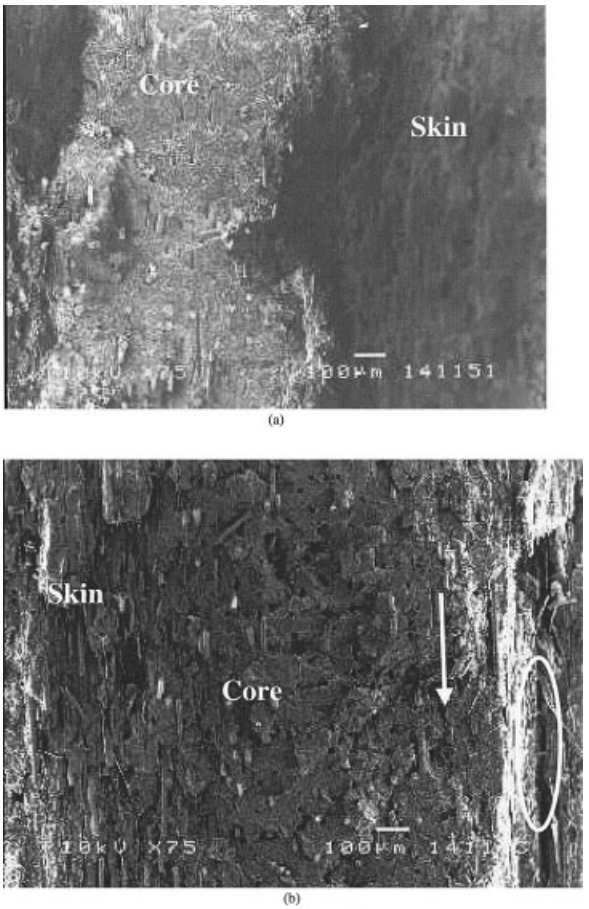

Figure 2 SEM images of the cryogenically fractured surface of N8G2L1. (a) The flow direction is perpendicular to the paper plane. (b) The flow direction is indicated by an arrow, and the thermal-shock-induced matrix cracks are marked with a white oval.

extensometer (strain gauge length = 12.5 mm) was mounted onto the specimens for strain measurements. Each specimen was monotonically loaded to failure, which was defined as the physical separation of the specimen, at a constant crosshead speed of 1 mm/min, according to ASTM standards for polymer-matrix composites. The fracture surfaces were examined with optical microscopes and SEM to examine the damage and to study the tensile-fracture behavior.

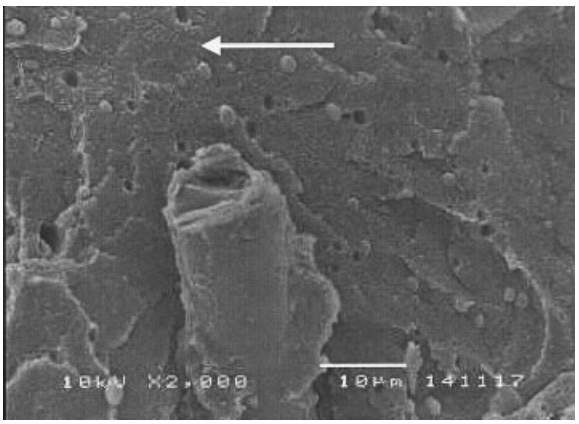

Figure 4 Spherical LCP droplets in the core region of N8G2L0.2 (indicated by an arrow).

RESULTS AND DISCUSSION

Morphology

All the injection-molded parts showed a distinctive skin–core structure. Two sets of SEM micrographs of cryogenically fractured surfaces of the composites are presented in Figures 1 and 2. Matrix cracks could be clearly observed between the skin and core regions in all of the samples and were believed to be a result of thermal shock. Two such cracks on the fracture surfaces of the hybrids are shown in Figures 1(a) and 2(b). A close examination of the fracture surfaces under SEM revealed many voids in the matrix, which were believed to be result of thermal expansion mismatch

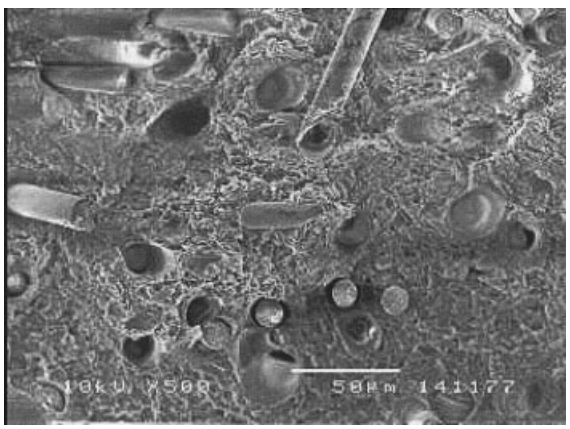

Figure 3 Poor fiber–matrix interface in N8G2.

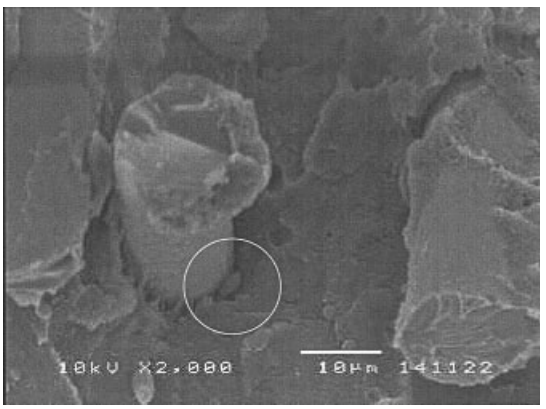

Figure 5 LCP droplets attached to E-glass fibers in the core region of N8G2L0.2 (indicated by a circle).

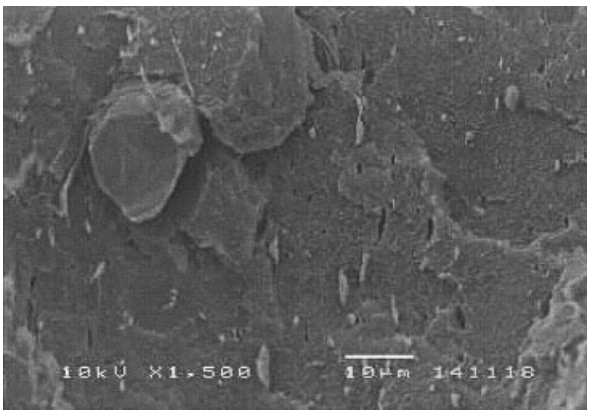

Figure 6 Ellipsoidal LCP phases in the skin region of N8G2L0.2.

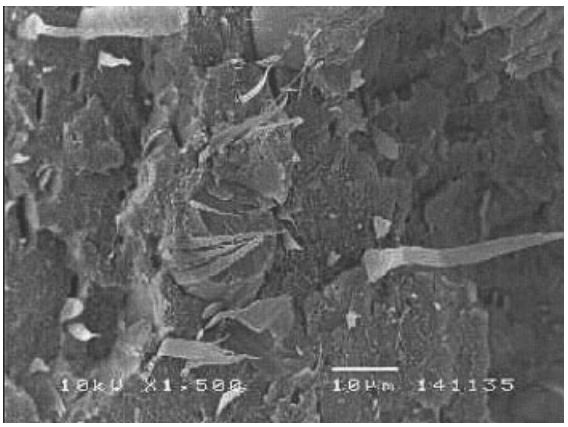

Figure 8 Ribbonlike LCP fibrils wrapping E-glass fibers in the skin region of N8G2L0.5.

between the constituents. On the fracture surface of plain short-E-glass-fiber composites (SGFCs; i.e., N8G2), crevices were seen between the glass fibers and matrix, indicating a poor adhesion of E-glass fibers to the matrix; therefore, fiber debonding and pullout were expected to happen easily. This is shown in Figure 3.

The shape of the LCP inclusions changed with an increase in the LCP content. When LCP content was increased to 1.96 wt % (at the same time, the E-glass-fiber content was reduced to 19.61 wt %) in N8G2L0.2; small, dispersed LCP phases could be observed, as shown in Figures 4–6. In the core region, most of these LCP inclusions were spherical droplets about 2 μm in diameter. They were not uniformly distributed within the matrix but seemed to gather near, or even directly attach to, E-glass fibers, as illustrated in Figure 5. This occurred because the hydrophilic E-glass fibers tended to be attracted by the polar amide group in the LCP chain. In the skin region, however, as shown in Figure 6, most LCP droplets were ellipsoids with longitudinal and transverse axes of about 5 and 1 μm, respectively. Occasionally, well-deformed LCP fibrils with higher aspect ratios could be found near E-glass fibers along the flow direction, as shown in Figure 7.

When the LCP concentration was increased to 4.76 wt % (the E-glass-fiber content was reduced to 19.05 wt %) in N8G2L0.5, although the majority of the dispersed LCP phases in the core region still remained spherical but had larger diameters, some of them were transformed into ellipsoids. In the skin region, more well-deformed LCP fibrils with higher aspect ratios could be seen, in comparison with those of the skin region of N8G2L0.2. Sometimes they even appeared as ribbonlike shapes, wrapping around E-glass fibers, as shown in Figure 8. Lamella-shaped LCP phases could also be found, some wrapping around the ends of E-glass fibers, as shown in Figure 9. This was believed to be a result of expanding flow at the gate, fountain

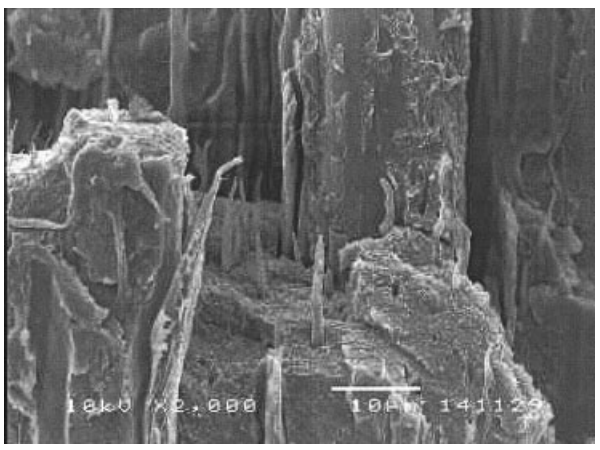

Figure 7 Well-deformed LCP fibrils in the skin region of N8G2L0.2.

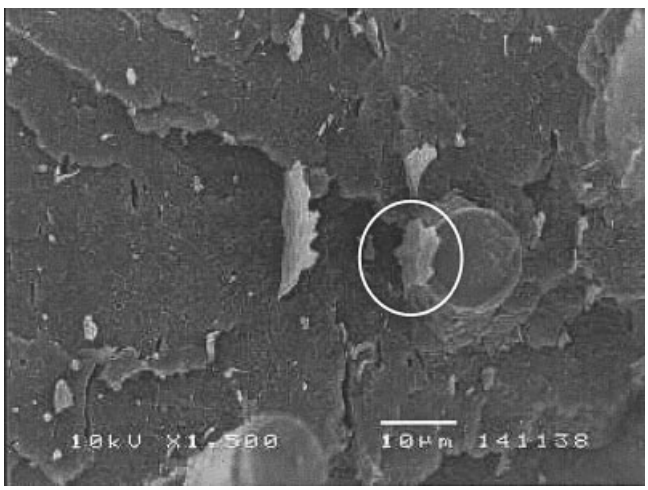

Figure 9 Lamella-shaped LCPs found in N8G2L0.5. Some of them are wrapping the end of the E-glass fibers (marked with a white ring).

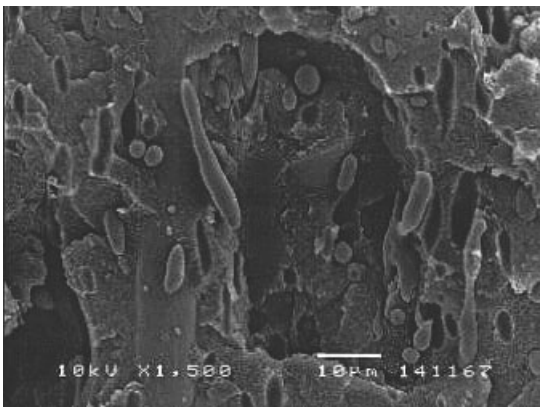

Figure 10 Ellipsoidal LCP phases found in the core region of N8G2L1. Some of them coalesce to form fibrillar structures.

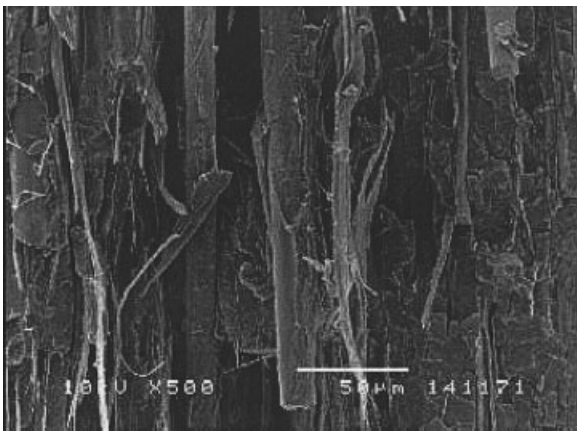

Figure 12 Long LCP fibrils found along E-glass fibers in the skin region of N8G2L1.

flow of the advancing melt, and nonisothermal shear flow, as suggested by He et al.[3]

When the LCP dosage was increased to 9.09 wt % (the E-glass-fiber dosage was reduced to 18.18 wt % concurrently) in N8G2L1, the majority of the LCP phases in the core region became ellipsoidal droplets, although few still retained their spherical form. Some of these LCP droplets coalesced to form fibrillar structures, as shown in Figure 10. Occasionally, this coalescence could generate large fibrils about 45 μm long and 4 μm in diameter (Fig. 11). In the skin region, almost all of the LCP phases existed in the form of fibrils, some of them with lengths comparable to that of E-glass fibers (Fig. 12). Like the previous case, there were also some ribbonlike LCP phases, sticking along or wrapping around E-glass fibers (Fig. 13).

With an increase in the LCP content, E-glass-fiber fragmentation was relieved. As stated earlier, the length of the E-glass fibers in this study was about 3 mm. However, as shown in the SEM images, only a small number of the glass fibers were still intact after the processing, with the majority of the fibers present in the specimens measuring only fractions of 1 mm, as shown in Figure 14; this was a result of severe shear stresses applied during extrusion and injection-molding. In comparison with the fragmentation the core region, the fragmentation of E-glass fibers was more severe in the skin region in an injection-molded part, whereas the scenario was most severe in plain SGFCs (i.e., N8G2) of all the composite systems. An SEM examination revealed that the fiber fragmentation was relaxed with the addition of LCP, and this was attributed to rheological changes. The mean fiber length dramatically increased from 119 μm for N8G2 to 271 μm for N8G2L0.2 after the incorporation of 1.96 wt % LCP and then steadily increased to 323 μm for N8G2L0.5 and to 385 μm for N8G2L1.

More fiber breakage was found in the skin region in which both the fiber concentration and shear stress were higher. Fiber breakage was mainly caused by

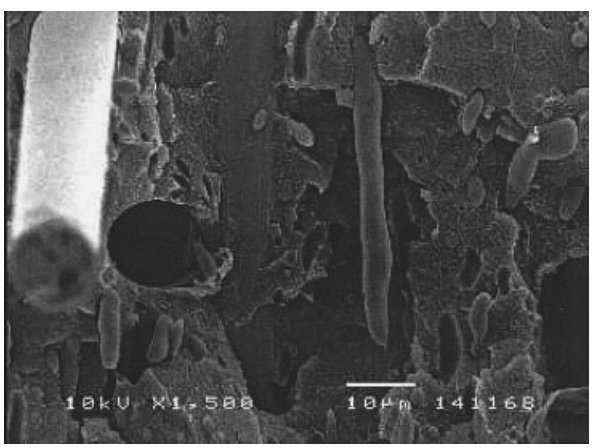

Figure 11 Big fibrillar structure, caused by the coalescence of LCP droplets, found in the core region of N8G2L1.

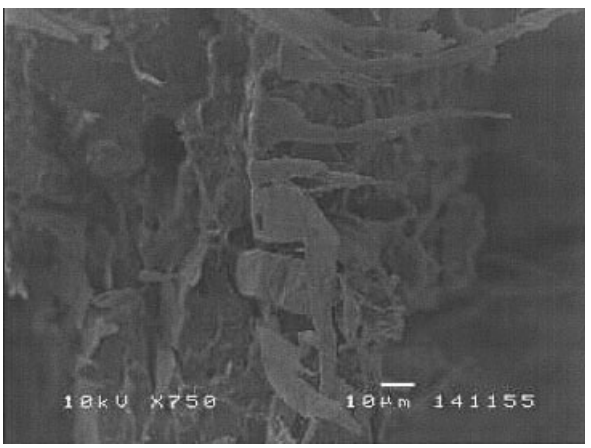

Figure 13 Wide, ribbonlike LCP phases found in the skin region of injection-molded parts of N8G2L1.

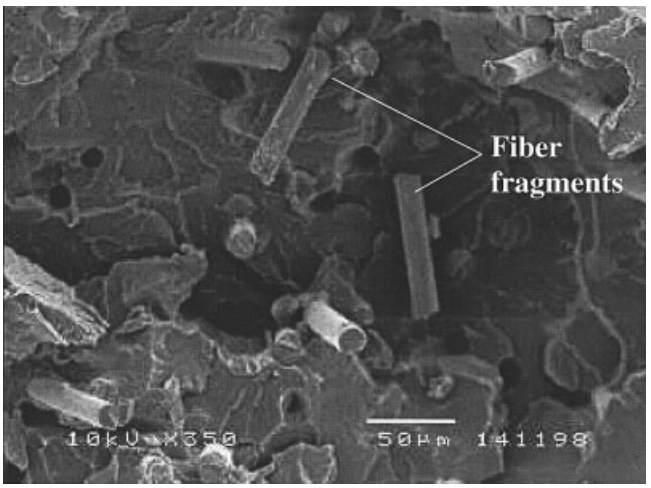

Figure 14 E-glass-fiber fragments observed in a cryogenically fractured N8G2 specimen.

excessive shear stress during extrusion and injection molding, which in turn was proportional to the viscosity of the melt. It has been suggested previously that the addition of LCPs to short-fiber-reinforced composites results in a reduction of the viscosity of molten blends.[5] Therefore, fiber breakage became less intensive with the addition of LCP, and this implied that the average aspect ratio of the primary reinforcement, that is, E-glass fibers, of the hybrid systems was higher than that of the plain SGFC.

Not only was E-glass-fiber breakage alleviated by an increase in the LCP content, but the glass-fiber alignment also was improved with the addition of LCP. A slight improvement in the E-glass-fiber alignment was observed with the addition of LCP, especially in the skin regions, upon a close examination of the samples. The mean value of the in-plane angles between the longitudinal axis of the glass fibers and the material flow direction decreased from 22.6° for N8G2 to 11.7° for N8G2L0.2, 11.0° for N8G2L0.5, and 3.2° for N8G2L1. This resulted from the intimation of E-glass fibers and LCP phases, which, with a lower viscosity (with respect to the polymer matrix) and a rigid chain structure, tended to align with the flow direction. Data on the LCP morphology, average glass-fiber length, and glass-fiber orientation are summarized in Table III.

The reinforcing effect of fibers in short-fiber-reinforced composites is dominated by the fiber orientation and fiber aspect ratio. Thus, less fiber breakage and improved fiber alignment brought by the addition of LCP result in improved mechanical properties for hybrid composite systems. However, the intimation of LCPs and E-glass fibers also corrupts the E-glass-fiber/matrix interface. For a tensile load to be transferred effectively to fibers, strong fiber–matrix adhesion is required. Therefore, the effect of interfacial

TABLE III
Quasistatic Tensile Properties of the Composites

Composition	UTS (MPa)	SD	Strain at break (%)	SD	Initial modulus (GPa)	SD	E-glass-fiber weight fraction (%)	LCP weight fraction (%)	Average glass-fiber length (µm)	Average glass-fiber orientation	LCP morphology	
											Core	Skin
N8G2	45.74	2.50	1.45	0.16	5.30	0.40	20	0	119	22.6	—	—
N8G2L0.2	46.93	2.51	1.46	0.28	4.76	0.14	19.61	1.96	271	11.7	Spherical	Ellipsoidal
N8G2L0.5	48.72	1.67	1.41	0.16	5.00	0.32	19.05	4.76	323	11.0	Spherical and ellipsoidal	Fibril
N8G2L1	50.06	2.75	1.36	0.12	5.24	0.31	18.18	9.09	385	3.2	Ellipsoidal and fibril	Long, ribbonlike fibril

SD = standard deviation.

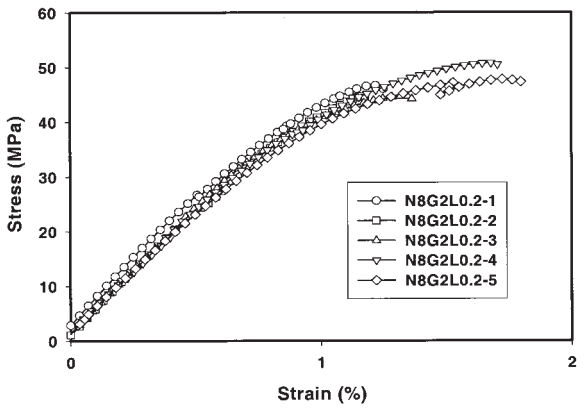

Figure 15 Typical stress–strain curves for N8G2L0.2.

degradation on the mechanical properties of the hybrid composite systems cannot be neglected.

Tensile behavior

Tensile test results obtained for the four different composite systems are tabulated in Table III. Each datum represents an average of at least four samples. All the samples displayed linear behavior up to 0.5% strains and then nonlinearity up to failure; this is typical for nonunidirectional short-fiber-reinforced composites. Some typical stress–strain curves are shown in Figure 15.

The ultimate tensile strength (UTS) of the composites is shown as a function of the E-glass-fiber weight fraction and LCP weight fraction in Figure 16. UTS of the composites decreased with an increase in the E-glass-fiber content but increased with an increase in the LCP content, almost linearly. The UTS increments upon the addition of LCP were 2.6, 6.4, and 8.6% when

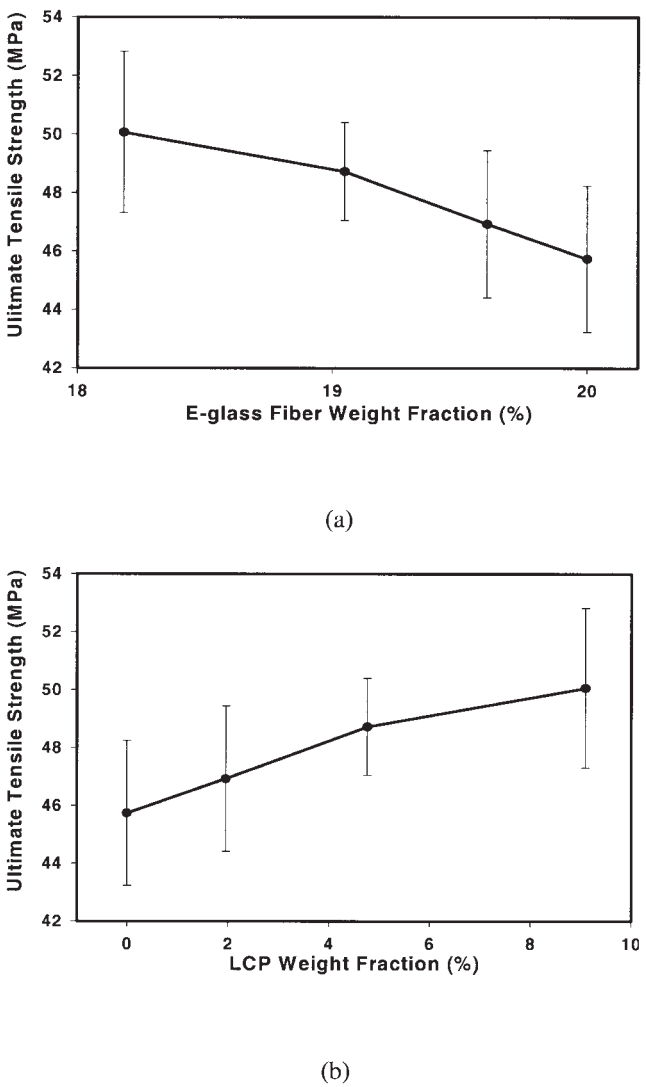

Figure 16 UTS as a function of the composition. The error bars indicate the range of the data.

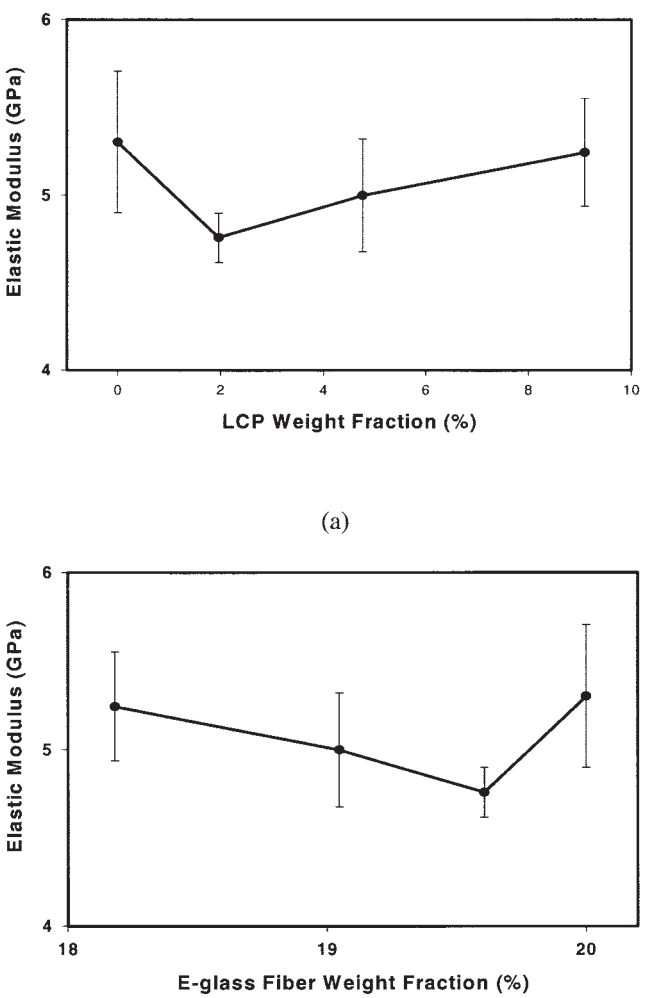

Figure 17 Elastic modulus as a function of the material composition. The error bars indicate the range of the data.

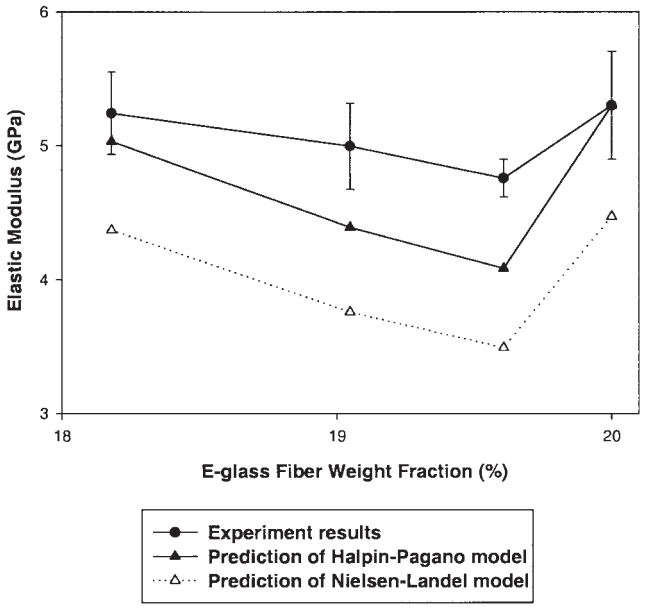

Figure 18 Comparisons of the model predictions and experimental results for the elastic modulus.

the weight percentage of LCP increased from 0 to 1.96, 4.76, and 9.09%, respectively.

A number of factors could affect the tensile behavior of the composites: (1) the variation of the constituents, (2) glass-fiber breakage, (3) glass-fiber alignment, (4) reinforcement by LCP, and (5) fiber/matrix-interface characteristics. With the addition of LCP, the aspect ratio and alignment of the E-glass fibers were enhanced, and the reinforcing effect of the dispersed LCP phase emerged. However, the interfacial adhesion between the E-glass fibers and matrix was weakened by the gathering of LCP phases along the glass fibers. Because the glass-fiber content was reduced at the same time, the increase in UTS upon the addition of LCP was the outcome of these competing mechanisms. Assuming that there were no other interfering mechanisms, we primarily attributed all of the UTS increments to the enhancement of the aspect ratio and alignment of the E-glass fibers because the volume fraction of the dispersed LCP phase was too low to be an effective load bearer. Considering the reduction of the glass-fiber content with the addition of LCP, we found that the increases in UTS were, in fact, substantial. If the surface properties of the E-glass fibers could be modified to promote adhesion to the matrix and their affinity with the LCP phases could be reduced, for example, by the addition of coupling agents, the tensile strength could be further improved. Therefore, from a material design perspective, optimization between the aforementioned mechanisms must be considered to realize the potential of this kind of material in strength-based designs.

The elastic modulus as a function of the E-glass-fiber and LCP contents is shown in Figure 17. The elastic modulus of the composites decreased from 5.30 (N8G2) to 4.76 GPa (N8G2L0.2); this was a 10% drop after the incorporation of 1.96 wt % LCP. With an increase in the LCP content from 1.96 to 4.76 to 9.09 wt %, the elastic modulus of the composites increased steadily, back to 5.24 GPa [N8G2L1; Fig. 17(a)]. A plot of the elastic modulus against the E-glass-fiber content is a mirror image of Figure 17(a). The deviation of the experimentally observed elastic modulus from the predictions of the rule of mixture, which essentially is a linear behavior, suggests a more complicated hybrid effect.

The reduction of the elastic modulus from 5.24 (E-glass-fiber content = 20 wt %) to 4.76 GPa (E-glass-fiber content = 19.61 wt %) partially reflected the reduced glass-fiber content. In addition, small LCP spheres congregated near and consequently corrupted the interface between the E-glass fibers and the matrix, hindered the stress transfer, and further lowered the elastic modulus. In this case, the improvements in the fiber alignment and orientation were minimal because of the relatively low LCP content. When more LCP was added, the positive influence on the stress transfer between the E-glass fibers and the matrix by improved fiber alignment and less fiber fragmentation began to outweigh the negative influence exerted by the corruption of the fiber–matrix interface and the reduction in the glass-fiber content. Moreover, the increase in the LCP content and the change in the geometry of the LCP inclusions also enabled them to contribute positively to the overall elastic modulus of the composites.

Predicting the stiffness of the composites

To model the elastic modulus of the composites, we assumed that both the glass fibers and LCP inclusions were evenly distributed throughout the composite and were perfectly bonded to the matrix and that no slip occurred between the different phases during

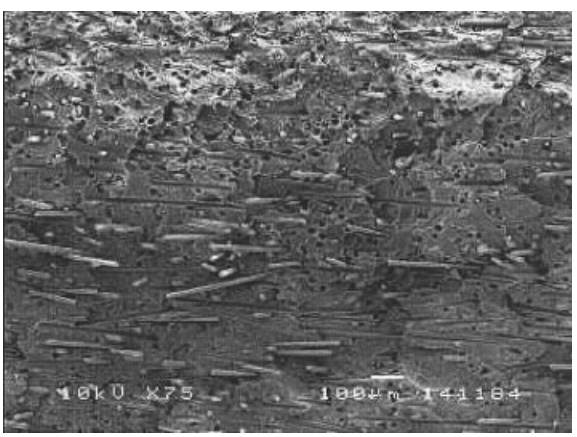

Figure 19 SEM micrograph of the tensile-fracture surface of N8G2L0.2.

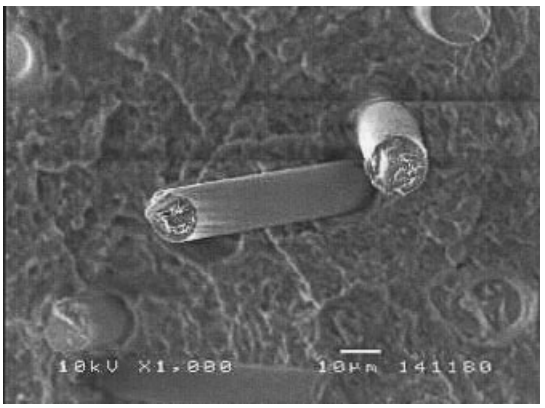

Figure 20 E-glass-fiber fractures observed on the tensile-fracture surface of N8G2.

loading. An injection-molded specimen was treated as a skin–core–skin laminate with no transit layer, with skin and core thicknesses of 0.5 and 1 mm, respectively. The average aspect ratio of the LCP inclusion was obtained by the random selection and measurement of 20 LCP inclusions under the SEM instrument from the skin and core layers of each composite. The aspect ratios of LCP were 5 (skin) and 1 (core) in N8G2L0.2, 10 (skin) and 1 (core) in N8G2L0.5, and 20 (skin) and 1 (core) in N8G2L1.

Here we adapt the model of Li and Narh[7] to estimate the elastic modulus of the LCP inclusions:

$$\ln\left(\frac{1}{E_f}\right) = -2.2722 + 0.1834\ln(X) + \ln(X)^2$$

where X is equal to η^{-2}, η is the aspect ratio, and E_f is the elastic modulus of the LCP inclusions. With this equation, the elastic moduli of the LCP inclusions with different aspect ratios in the hybrid systems could be calculated. The stiffness of the plain SGFC (N8G2) could be calculated directly with the Halpin–Tsai model for unidirectional short-fiber composites, and this was followed by the Halpin–Pagano extensional model for two-dimensional, randomly oriented short-fiber composites[8] or the Nielsen–Landel model for three-dimensional, randomly oriented short-fiber composites.[9] A layer of the hybrid composite (skin or core) was treated as a separate lamina, exhibiting in-plane isotropy. Each layer was treated as a randomly oriented, short-glass-fiber-reinforced *in situ* composite. This enabled us to calculate the overall stiffness of the layer with the Halpin–Tsai model, the Halpin–Pagano model, or the Nielsen–Landel model by obtaining the stiffness of the virtual matrix first and then the hybrid composite. Subsequently, the stiffness of the coupons could be calculated through the assembling of the layers together with the rule of mixture for laminates. With material data provided by the vendors (the modulus of Noryl was 2.105 GPa, as measured with tests on neat Noryl coupons fabricated with the same procedures used in this study), the obtained results are shown in Figure 18. Although predictions by the Halpin–Pagano model agreed excellently with the experimental results for plain SGFC (N8G2) and the *in situ* hybrid composite with the highest LCP concentration (N8G2L1), the predictions for N8G2L0.2 and N8G2L0.5 were lower than the experimental results. The values predicted by the Nielsen–Landel model were lower than the experimental results. Interestingly, the predictions of both methods showed the same patterns as the experimental results. However, the apparent agreement only indicated a stiffness change caused by changes in the fraction and geometry and hence the properties of the reinforcement. Nonetheless, these models could provide conservative estimates of the elastic properties of the material.

Tensile failure mechanisms

SEM micrographs of the tensile-fracture surfaces are presented in Figures 19 and 20. Prominent fiber pullout occurred in all the samples (Fig. 19). Although fractures of E-glass fibers could also be observed, as shown in Figure 20, the interfacial failures, such as fiber debonding, and subsequent fiber pullout contributed significantly to the overall failure mechanism. An islandlike fracture surface, an indication of multidirectional crack propagation, was seen in some of the samples. This was believed to be a result of the weak E-glass-fiber/matrix and LCP/matrix interfaces. The propagating matrix crack could have been easily deflected at these places instead of traveling in a straightforward manner. With the addition of LCP, different forms of LCP inclusions emerged. Because of substantial thermal expansion mismatch between the LCP and

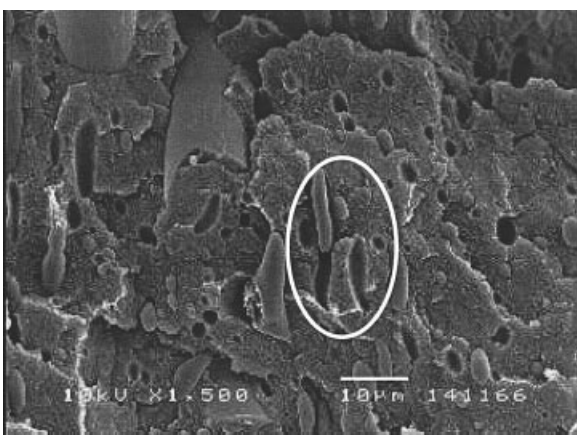

Figure 21 LCP retracting into the core region of injection-molded parts of N8G2L1 (marked by a white oval).

matrix, when the composites parts were cooled to the ambient temperature at the end of processing, the LCP inclusions contracted, as shown in Figure 21, thus weakening the LCP/matrix interface and sometimes even debonding themselves from the matrix, leaving matrix voids (this happened more extensively in the core regions).

The hierarchical structure of LCP–glass–matrix composites is expected to be positively beneficial. Although LCP inclusions are considered secondary reinforcements, they are expected to act not as the major load bearers but as crack arresters to block the propagation and coalescence of microcracks. However, morphological studies have revealed that, although the presence of LCP improves glass-fiber alignment, reduces fragmentation, and provides reinforcement to the matrix, its presence also weakens the interface between the E-glass fibers and matrix and results in a more porous matrix with microvoids acting as stress raisers.

CONCLUSIONS

According to a morphological study, the *in situ* hybrid systems have a hierarchical microstructure containing reinforcements with size differences as high as two orders of magnitude. With an increase in the LCP content, the geometry and dimensions of the LCP phase inside the composites changes, from spherical droplets to ellipsoidal droplets and then to fibrils or lamellar structures. The alignment of E-glass fibers is improved and fiber breakage is less intensive with the addition of LCP. However, these potential benefits and the emerging reinforcing effect of LCP seem to be offset by the affinity of LCP to E-glass fibers, which weakens the E-glass-fiber/matrix interface and stress raisers generated by LCP as a result of thermal mismatch. These competing mechanisms result in a moderate increase in the tensile strength and a more complicated pattern of the tensile elastic modulus of the composites with the addition of LCP, despite reduced glass-fiber content. Tensile fractography analysis has indicated that the tensile fractures in the composites are dominated by interfacial failure. To enhance the performance of this kind of material for engineering applications, the interfacial adhesion between the reinforcements and the matrix must be further improved.

References

1. Hayashi, T. Fukugo Zairyo 1972, 1, 18.
2. Hayashi, T. Proceedings of the 8th International Reinforced Plastics Conference; British Plastics Federation: London, 1972.
3. He, J. S.; Bu, W. S.; Zhang, H. Z. Polym Eng Sci 1995, 35, 1695.
4. He, J. S.; Wang, Y. L.; Zhang, H. Z. Compos Sci Technol 2000, 60, 1919.
5. He, J. S.; Zhang, H. Z.; Li, G.; Xu, X. Acta Polym Sinica 1993, 1, 115.
6. He, J. S.; Zhang, H. Z.; Wang, Y. L. Polymer 1997, 16, 4279.
7. Li, Z.; Narh, K. A. Compos B 2001, 32, 103.
8. Halpin, J. C.; Pagano, N. J. J Compos Mater 1969, 3, 720.
9. Nielsen, L. E.; Landel, R. F. Mechanical Properties of Polymers and Composites; Marcel Dekker: New York, 1994.